CrossMark

Automatic estimation of midline shift in patients with cerebral glioma based on enhanced voigt model and local symmetry

Mingyang Chen[1,2] · Ahmed Elazab[1,2] · Fucang Jia[1,2] · Jianhuang Wu[1,2] ·
Guanglin Li[1,2] · Xiaodong Li[3] · Qingmao Hu[1,2]

Abstract Cerebral glioma is one of the most aggressive space-occupying diseases, which will exhibit midline shift (MLS) due to mass effect. MLS has been used as an important feature for evaluating the pathological severity and patients' survival possibility. Automatic quantification of MLS is challenging due to deformation, complex shape and complex grayscale distribution. An automatic method is proposed and validated to estimate MLS in patients with gliomas diagnosed using magnetic resonance imaging (MRI). The deformed midline is approximated by combining mechanical model and local symmetry. An enhanced Voigt model which takes into account the size and spatial information of lesion is devised to predict the deformed midline. A composite local symmetry combining local intensity symmetry and local intensity gradient symmetry is proposed to refine the predicted midline within a local window whose size is determined according to the pinhole camera model. To enhance the MLS accuracy, the axial slice with maximum MSL from each volumetric data has been interpolated from a spatial resolution of 1 mm to 0.33 mm. The proposed method has been validated on 30 publicly available clinical head MRI scans presenting with MLS. It delineates the deformed midline with maximum MLS and yields a mean difference of 0.61 ± 0.27 mm, and average maximum difference of 1.89 ± 1.18 mm from the ground truth. Experiments show that the proposed method will yield better accuracy with

the geometric center of pathology being the geometric center of tumor and the pathological region being the whole lesion. It has also been shown that the proposed composite local symmetry achieves significantly higher accuracy than the traditional local intensity symmetry and the local intensity gradient symmetry. To the best of our knowledge, for delineation of deformed midline, this is the first report on both quantification of gliomas and from MRI, which hopefully will provide valuable information for diagnosis and therapy. The study suggests that the size of the whole lesion and the location of tumor (instead of edema or the sum of edema and tumor) are more appropriate to determine the extent of deformation. Composite local symmetry is recommended to represent the local symmetry around the deformed midline. The proposed method could be potentially used to quantify the severity of patients with cerebral gliomas and other brain pathology, as well as to approximate midsagittal surface for brain quantification.

Keywords Deformed midline · Cerebral glioma ·
Mechanical model · Local symmetry · Magnetic resonance imaging

Introduction

Midline shift (MLS, which is the deformation of midline) is the most important quantitative feature for clinicians to evaluate the severity of brain compression caused by space-occupying lesions such as hemorrhage and tumor, for diagnosis and prognosis [1]. Cerebral glioma is one of the most aggressive space-occupying diseases with incidence around five to ten per 100,000 general population [2]. Magnetic resonance imaging (MRI) is commonly used

✉ Qingmao Hu
  qm.hu@siat.ac.cn

1   Shenzhen Institutes of Advanced Technology, Chinese
    Academy of Sciences, Shenzhen, China

2   University of Chinese Academy of Sciences, Beijing, China

3   Linyi People's Hospital, Linyi, China

 Springer

for early diagnosis of gliomas [3]. Researches manifest that the presence of MLS is an important prognostic factor influencing survival [4]. While considerable attentions have been paid on MLS quantification of hemorrhage patients, there is no existing literature on quantification of cerebral gliomas. Tumor and edema are two major pathological factors influencing MLS for patients with cerebral gliomas [5]. Quantification of MLS for hemorrhage patients is based on computed tomography images and thus could not be directly applicable to patients with gliomas. Hence, an efficient method to compute MLS for patients with gliomas from MRI is desirable.

So far, researches on quantification of MLS are concentrated on traumatic brain injury [1, 6–11]. These methods could be classified as: symmetry-based [1], regression model based [6], and anatomical markers based [7–11]. Liao et al. [1] employed a quadratic Bezier curve to approximate the deformed midline (dML) with three segments: the upper and lower line segments of the falces, and the middle curved segment formed by the intervening brain using the traditional local intensity symmetry. Liu et al. [6] measured MLS based on a linear regression model for the relationship between the hemorrhage and the MLS and adjusted according to local intensity symmetry. Anatomical markers based methods assume the existence of feature points on the dML: falx, septum pellucidum (SP), and the center of third ventricle. Xiao et al. [7, 8] approximated MLS from SP by combining multiresolution binary level set segmentation [9] and Hough transform. Chen et al. [10] applied a set of ventricle templates based on which the MLS was estimated to match feature points. Liu et al. [11] estimated the dML as the 3 line segments connecting 4 anatomical markers (the frontal falx, center of the frontal horn of lateral ventricle, center of the third ventricle, and lateral falx).

As noted in [7], symmetry-based methods might fail for cases with symmetry destroyed by pronounced brain compression. The regression model cannot be well suited to individual data due to the complexity of deformation and the nature of regression. Anatomical markers based methods [7–11] will fail when the markers are absent (such as the SP in [7]) or the model to determine the markers is not always valid (such as the model for falces in [11] and SP in [7]).

The maximum MLS is known as most relevant measurement for quantifying pathology severity. In fact, the maximum MLS might not always occur at the axial slice containing SP and third ventricle as did in [1, 6–11]. Thus, to identify the axial slice with maximum MLS is desirable.

Viscoelasticity is a significant measure of the microstructural constitution of soft biological tissue. In viscoelastic theory, the stress–strain relationship is usually modeled by a combination of elastic and viscous elements for characterizing the specific rheological behavior (i.e.

viscoelastic deformation) of the material [12]. Numerical studies show that the brain tissue deformation should be approximated by non-linear-viscoelastic model [13–15] rather than simple linear or quadratic curve model [1, 6]. Voigt model is frequently used in the literature [16], which is mainly applied in image registration for surgery plan and intraoperative navigation [17].

In this paper, we investigate approximation of MLS on axial slices by combining mechanics model and features of image symmetry. More specifically, an enhanced Voigt model is proposed to simulate the midline deformation after cerebral gliomas to predict the dML. A new way to define local symmetry based on intensities and intensity gradients is explored for the mechanical model to be tailored to the image features to refine the dML. The issues of finding the appropriate axial slice and robust determination of falces are also addressed. The preliminary results of this study have been presented as an oral lecture at the 29th International Congress and Exhibition on Computer Assisted Radiology and Surgery (2015) in Barcelona, Spain.

Materials and methods

Materials

Thirty subjects from the Virtual Skeleton Database (https://www.virtualskeleton.ch/BRATS/Start2013) are used for this study. All subjects are provided from the Multimodal Brain Tumor Segmentation challenge organized by the MICCAI 2013 conference. The data contain multi-contrast MRI scans of 10 low- and 20 high-grade glioma patients that have been manually annotated with four lesions labels (necrosis, edema, non-enhanced tumor, and enhanced tumor). The ground truths of the tumor and the edema regions were manually delineated by clinical experts of MICCAI conference and could be accessible from the website (http://martinos.org/qtim/miccai2013/index.html). For each subject, the data include T1, T2, FLAIR, and post-Gadolinium T1 magnetic resonance volumes. All volumes have been skull stripped, linearly co-registered to T1 contrast volume, and interpolated to 1 mm isotropic resolution. In this study, only the T2 volume of each subject is used for delineating dML. The ground truths of the MLS were determined by a clinical expert from Linyi People's Hospital on both the original and interpolated axial slices (with spatial resolution of 1 and 0.33 mm respectively).

Methods

The proposed method consists of three components: preprocessing, prediction and refinement of dML. The

preprocessing component is to determine the midsagittal plane (MSP), find the representative axial slice to quantify the MLS, rotate the axial slice and interpolate the representative axial slice. The prediction component is to determine the initial dML using enhanced Voigt model iteratively. The refinement component is to construct the local symmetry metric, refine and smooth the predicted dML. These components are detailed below.
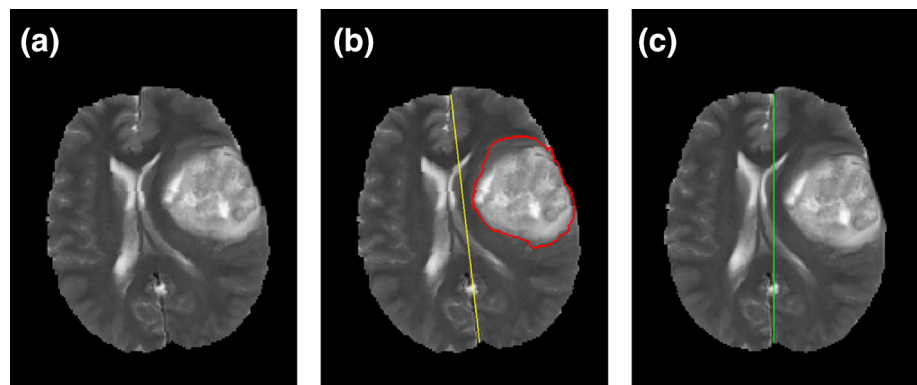
Preprocessing

The axial slice with maximum MLS is manually picked for each data. Its automation is elaborated in Discussion section.

The MSP is extracted based on local symmetry and outlier removal [18] (Fig. 1b, yellow line).The ideal midline (iML) of an axial slice is obtained by connecting two intersections between the MSP and the brain boundary. Each scan is rotated to make iML vertical for facilitating subsequent processing (Fig. 1c, blue line).

The frontal and lateral falces are the starting and ending points of both iML and dML segments which will not deform due to pathology. It is thus desirable to determine the two falces based on a methodology that can get rid of the influence of pathology. Since the MSP is determined as if there were no pathology due to outlier removal [18], the intersection points between the MSP and the brain boundaries of the axial slice are taken as the two falces (Fig. 1c, the end points of the green line segment).

As the spatial resolution of the axial slice is 1 mm, which is much lower than the spatial resolution of computed tomography axial slice (around 0.30 mm per voxel) for determining MLS, the rotated axial slice is then interpolated 3×3 using a bicubic interpolation scheme to have a new spatial resolution of 0.33 mm per voxel in both X and Y directions. The subsequent processing is based on the rotated and interpolated axial slice. The dependency of MLS accuracy on the interpolated spatial resolution is elaborated in the Discussion section.

Prediction of the deformed midline

In this section, the original Voigt model is first introduced, followed by construction of an enhanced model according to the analysis of the viscoelastic properties of brain tissues.

(1) *The original Voigt model* The viscoelasticity of brain tissues can be described intuitively as consisting of an ideal spring (to simulate the ordinary spring deformation whose mechanical properties follow the Hooke's law) and dashpot (to simulate the viscous deformation which obeys the laws of Newtonian fluid) [19]. The Voigt model is employed to describe the viscoelastic properties of brain tissue due to its good fitting of the property of the deformation of brain tissues corresponding to the creep curve of the Voigt model [20].The relationship between the strain ε and stress σ(Pa) could be described by the following equation:

$$\sigma = K\varepsilon + \mu \frac{d\varepsilon}{dt} \qquad (1)$$

where K (Pa) is the elastic coefficient of the ideal spring, and μ(Pa.sec) is the viscosity coefficient of the ideal dashpot. The solution is

$$\varepsilon(t) = \frac{\sigma}{K}\left(1 - e^{-t/\tau}\right) \qquad (2)$$

where $\tau = \frac{\mu}{K}$ is the relaxation time (sec).

(2) *Construction of the enhanced Voigt model* The dML can be influenced by at least the following 4 factors: the size of the lesions (larger size will yield greater amount of MLS), the distance between the lesion and the iML (longer distance will yield smaller amount of MLS), the elastic property of midline points (those further apart from the skull are easier to deform), and the rigidity of the skull (points with smaller distance to the skull will deform less).

To account for these factors, the stress in Eq. (2) is adjusted to construct an enhanced Voigt model. In particular, the gravity $G(P, Q)$ (N) between voxel

Fig. 1 An axial slice (**a**), the brain and the delineated lesions (region enclosed within the *red* contour) (**b**), and the rotated brain with the ideal midline (*green line segment*) being vertical (**c**)

Q on the iML and the lesion is used to indirectly represent the pressure of the lesion

$$G(P, Q) = \frac{gM_P M_Q}{r^2} \qquad (3)$$

where P is the geometric center of the lesion, M_P and M_Q(kg) are respectively the mass of the lesion and Q, r(m) is the Euclidean distance between P and Q, and g(Nm^2/(kg)^2) is the gravitation constant (Fig. 2). In addition, a positional harmonic item $F(r)$(1/m^2) is introduced to account for the positional constraint with variable rigidity,
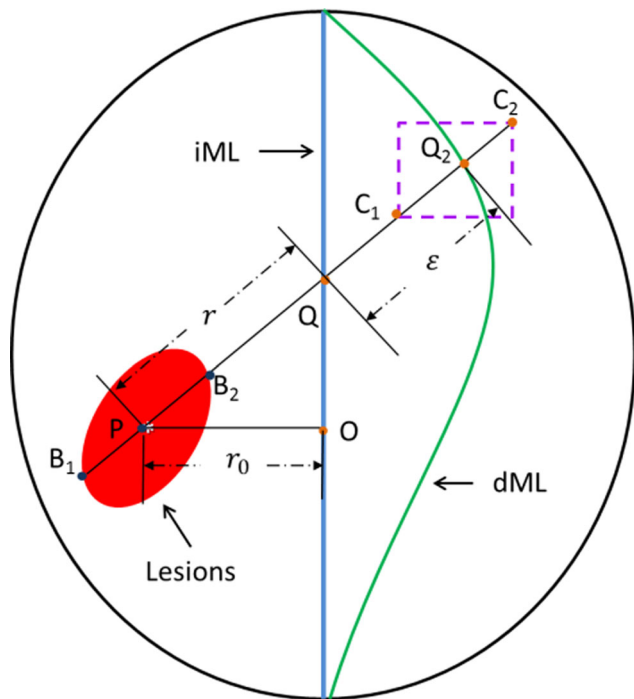
$$F(r) = A\left(1 - \frac{1}{\sqrt{2\pi}\delta}\exp\left(-\frac{(r - r_0)^2}{2\delta^2}\right)\right) \qquad (4)$$

where r_0(m) is the distance from P to the iML, δ is the standard deviation of the distances between P and all voxels on the iML, and A is the modulation factor in the range $[5 \times 10^{-5}, 4.5 \times 10^{-3}]$. The stress after adjustment is

$$\sigma = F(r) \times G(P, Q) \qquad (5)$$

The eventual constitutive equation of the enhanced Voigt model is thus,

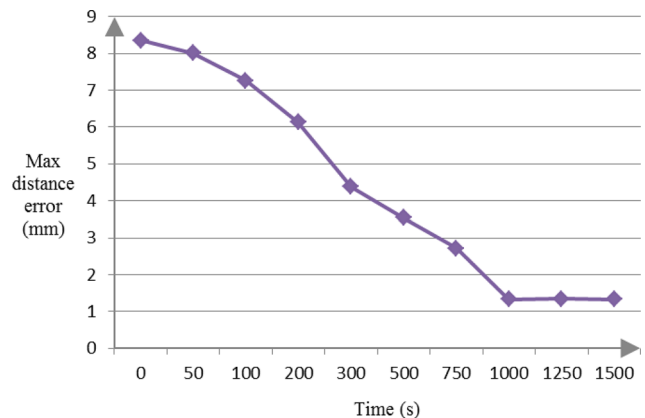$$\varepsilon(r, t) = \frac{F(r)gM_P M_Q}{Kr^2}\left(1 - e^{-t/\tau}\right) \qquad (6)$$

(3) *Parameters assignment* The geometric center P and voxel Q in Eq. (6) correspond to two particles with masses:M_P = the number of the voxels of the lesion and $M_Q = 1$ (kg). The geometric center P is derived from tumor voxels (see Discussion for justification). The elastic coefficient and the viscosity coefficient of brain tissue are set from literature [21] as follows: $K = 6.67 \times 10^{-4}$(Pa), and $\mu = 0.0075$(Pa.sec). The gravity constant g is 1 (Nm^2/(kg)^2).

As shown in Eq. (6), the strain changes with time, while the dML to be extracted is a static state at a certain time instant. Thus, we assume that the dML has reached the stable state when the MRI scans are obtained. Experiments with varying t in [1, 1500] (sec) are carried out to find that a value of not smaller than 1000 (sec) is appropriate. The curve of error evolution corresponding to parameter t is shown in Fig. 3.
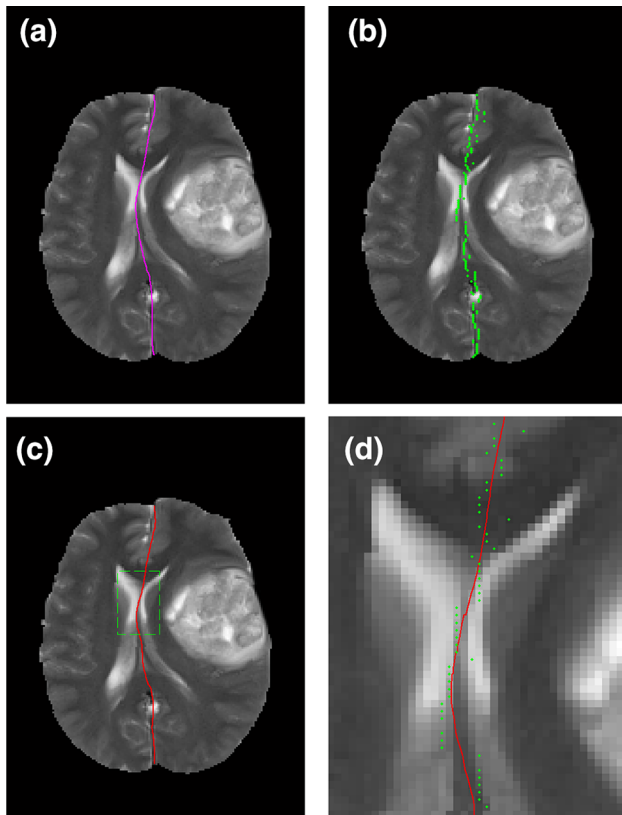
(4) *Prediction* The initial strains of all voxels on the iML are approximated in this step. According to the strong rigidity of the cerebral dura matter, we consider the segments of the first one-twelfth from the top and the last one-fourth of the iML as the falx segment, and the positional harmonic item $F(r)$ is set as the minimum of $F(r)$, i.e., $A\left(1 - \frac{1}{\sqrt{2\pi}\delta}\right)$. For the remaining voxels on the iML, $F(r)$ is computed according to Eq. (4). An example of the predicted dML is shown in Fig. 4a (purple curve).

Composite local symmetry

As pointed out by Davidson and Hugdahl [22], the brain exhibits rough local symmetry around the midline. Resorting to local symmetry to refine the predicted dML seems reasonable. Unlike most existing methods which only employ the intensity information to describe the local

Fig. 2 The sketch map of the *midline* shift of the enhanced Voigt model and determination of local neighborhood for dML refinement

Fig. 3 The *curve* of error evolution with respect to parameter t

Fig. 4 The predicted dML (**a**), points with maximum composite local symmetry within the neighborhood of predicted dML (**b**), the eventual dML after *curve* smoothing (**c**), and magnified points with maximum local symmetry of (**b**) (*green points*) and the corresponding *curve* after smoothing within the *green window* of (**c**) (*red curve*) (**d**)

symmetry, both intensities and intensity gradients are exploited to form the composite local symmetry that intends to enhance the local symmetry contrast of voxels both in the uniform and non-uniform region around dML.

(1) *Local intensity symmetry* Denote the intensity of a voxel at (x,y) as $f(x, y)$, and the coordinates of a voxel P as (x_p, y_p). The traditional expression of local intensity symmetry is the sum of absolute intensity differences for pairs of voxels along the line segment perpendicular to dML. Since the iML has been rotated to be vertical, the initial local intensity symmetry can be approximated along the horizontal direction. All voxel within its neighborhood N_p (7×7) will be involved to calculate the initial local intensity symmetry of a voxel P. Suppose voxel q is within N_p and its mirror voxel with respect to p is q'. The initial local intensity symmetry SD is calculate as

$$SD(p) = \sum_{q \in N_p} \left| f(x_q, y_p) - f(x_{q'}, y_p) \right| e^{-\frac{(q-p)^2}{2}} \quad (7)$$

One potential problem of SD in Eq. (7) is that voxels in a region with uniform intensities could also be

small, which makes it difficult to differentiate from its neighboring voxels. A Gaussian filtering in vertical direction is employed to enhance the intensity symmetry contrast. The modified SD map could then be detected through edge detection such as a Laplacian-of-Gaussian (LOG) filter [23]. The local intensity symmetry can then be defined as

$$SS = (SD * Gauss) * LOG \quad (8)$$

where $*$ is for convolution, and *Guass* is for Gaussian filter (mean being 0, and standard deviation being 0.5).

As shown in Fig. 5, SS of the voxels on the symmetry curve in regions with uniform intensities tends to be maximal due to the introduction of Gaussian filtering and LOG (the red curve), which will not be discernable from neighborhood voxels if LOG is not employed (the blue curve).

(2) *Local intensity gradient symmetry* As is pointed out [24], the gradient information is more discriminative than intensity, and more stable to photometric changes [24]. Inspired by SIFT [25], HOG [26], and the method proposed by Hauagge and Noah [27], a histogram of local intensity gradient orientations $h(q)$ at each voxel q is constructed from the intensity gradient magnitude $M(x, y)$ and orientation $\theta(x, y)$ (in the range of 0 to π) with a gradient operator such as Sobel operator.

The orientation of voxels (Dir) within N_q (7×7) are grouped into an orientation histogram with 8 bins, i.e., $[0, \pi/8)(Dir_0)$, $[\pi/8, \pi/4)(Dir_1)$, …, and $[7\pi/8, \pi](Dir_7)$, weighted by the gradient magnitude of voxels within N_q. The gradient orientation histogram $\hat{h}_q(Dir_j)$ is thus calculated as follow:

$$\hat{h}_q(Dir_j) = \sum_{\substack{\theta_i \in Dir_j \\ i \in N_q}} M_i(\theta_i) \quad (9)$$

where $j = 0, 1, 2, \ldots, 7$, θ_i and M_i are the gradient orientation and the gradient magnitude of voxel i.

The histogram $\hat{h}_q$ is normalized to form the final gradient orientation histogram:

$$h_q(Dir_j) = \frac{\hat{h}_q(Dir_j)}{\sum_{j=0}^{7} \hat{h}_q(Dir_j) + \xi} \quad (10)$$

where ξ is a constant (0.05) used to enhance the robustness to noise.

If voxels q and q' are symmetrical to dML in terms of both position and local intensity distribution, histogram h_q should be similar to the reflected

Fig. 5 Illustration of the difference between local symmetry of the voxels in the region (*green line*) with uniform intensities for SD (*blue curve* in (**d**)) and SS (*red curve* in (**d**)), where the location of the *arrow* is the symmetry center. Figure 5b, c are respectively the SD and SS images of Fig. 5a
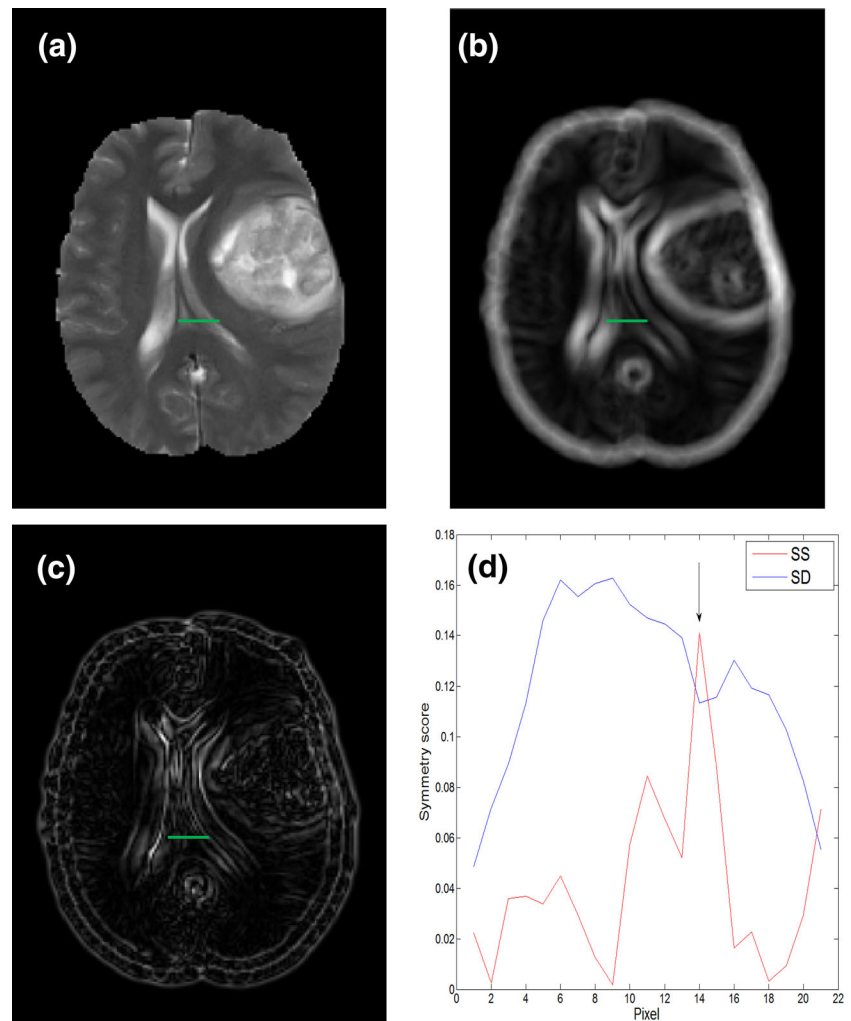
histogram of q' which is denoted as $h'(q')$. A possible way to quantify the similarity of intensity gradients of two voxels q and q' is to define the metric as dot product of the two vectors h_q and $h'(q')$. The intensity gradient symmetry $SG(p)$ is calculated as:

$$SG(p) = \sum_{q \in N_p} h(q) \circ h'(q') e^{-\frac{(q-p)^2}{2}} \qquad (11)$$

where $\circ$ is dot production of vectors. It can be shown clearly that SG will be maximized when q and q' are a pair of symmetric intensity gradient voxels (Fig. 6).

(3) *The composite local symmetry* The composite local symmetry metric Sym is defined as:

$$Sym = SS' \times (1 - grad) + grad \times SG' \qquad (12)$$

where $grad$ is the normalized gradient magnitude $M(x, y)$, SS' and SG' are respectively the normalized SS and SG with range [0, 1]. It can be shown that the greater the Sym of a voxel p, the bigger the

probability of the voxel to be on the dML: the local intensity symmetry will be dominant ($Sym \approx SS'$) when the voxels belong to uniform regions with weak edge information (i.e., $(1 - grad) > > grad$); the local gradient symmetry will be dominant ($Sym \approx SG'$) when the voxels belong to non-uniform regions with strong edge information (i.e., $grad > > (1 - grad)$). Figure 7a, b, c show respectively SS, SG and the Sym of Fig. 1a.

With different modulation factor A, the sum of composite local symmetry on the dML can be calculated. The eventual dML will be the one with maximum sum of composite local symmetry to be refined.
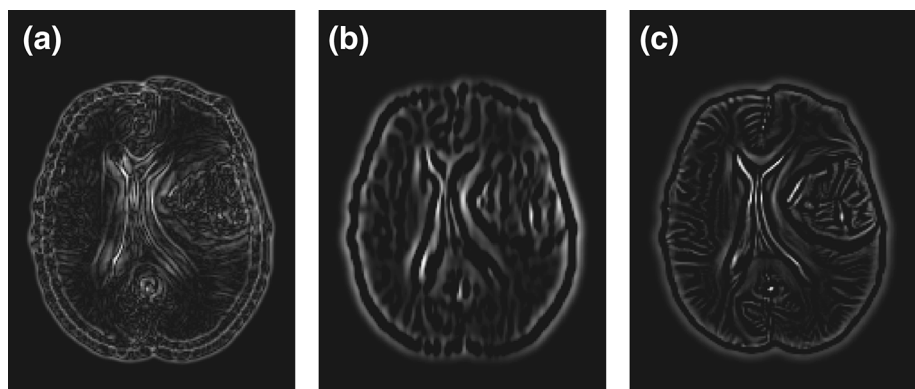
Refinement based on local symmetry

The deformation of midline is caused by multi-factors besides lesions such as imaging time and inhomogeneity of
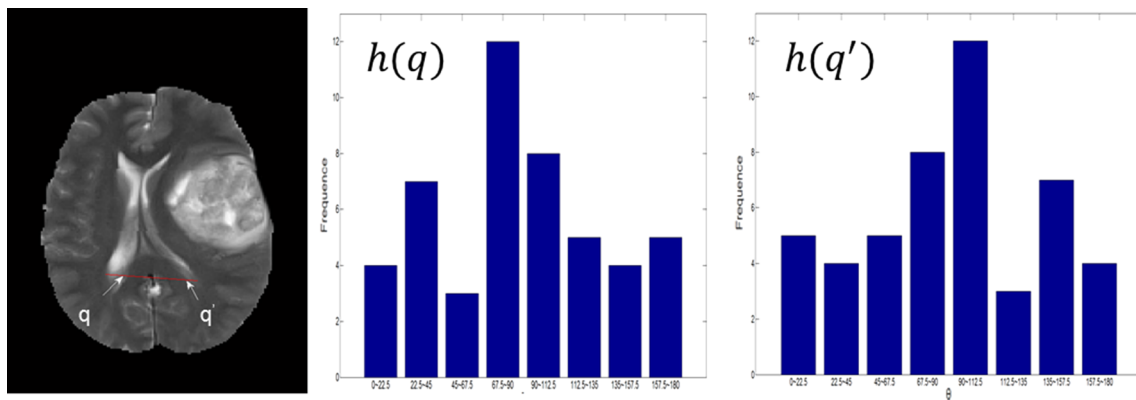
Fig. 6 Two gradient orientation *histograms* of a voxel-pair being symmetric in terms of both position and local gradient distribution with respect to dML

Fig. 7 Images of the local symmetry (**a**) SS, (**b**) SG, and (**c**) Sym of Fig. 1a

the viscoelasticity of different brain tissues. Thus, it is necessary to adjust the predicted dML according to image features. The refinement is to include: determination of local neighborhood and refinement of dML within the local neighborhood according to the composite local symmetry.

(1) *Determination of local neighborhood* The local neighborhood of the predicted dML is a rectangle inspired by the pinhole camera model determined in the following way. For any voxel Q on the iML, we connect points P and Q, and extend the line segment PQ to get two intersection points (B_1 and B_2) on the lesions boundary (Fig. 2). The mirror points C_2 and C_1 of the points B_1 and B_2, respectively, are obtained by using the predicted strain ε computed from Eq. (6) as the focal length and the point Q as the pinhole.

(2) *Refinement according to local symmetry and curve smoothing* For each voxel P on the predicted dML, the voxel with maximum composite local symmetry Sym within the local rectangular neighborhood of P is searched to replace the predicted voxel P (Fig. 4b). Denote the coordinates of these voxels

as $p_i(x_i, y_i)$ and the voxels p_i' after smoothing as (x_i', y_i') $(i = 1, 2, \ldots, N)$, where N is the number of voxels of the predicted dML. We fix the first and last points on both the predicted and eventual dMLs to be the intersection points between the MSP and the brain boundaries of the axial slice. The following rules are employed to find voxels (x_i, y_i) with maximum local symmetry to replace the predicted dML:

(a) If there is only one voxel p_i with the maximum local symmetry, p_i is chosen to replace the voxel P;

(b) If there is more than one voxel with the same maximum local symmetry, the point closest to the last optimal point p_{i-1} is chosen to replace the voxel p.

A simple average of p_{i-2}, p_{i-1}, p_i, p_{i+1}, and p_{i+2} is implemented to smooth the coordinates to derive p_i' with coordinates (x_i', y_i')(Fig. 4d). Finally, the approximated dML is obtained by connecting voxels p_i' and p_{i+1}' $(i = 1, 2, \ldots, N-1)$ (Fig. 4c).

The complete procedure to approximate dML is summarized in Table 1.

Results

The dML error of a voxel on the approximated dML is defined as the minimum distance between this voxel and all the voxels on the ground truth dML. To evaluate the performance of the proposed method, the following measures are employed: the mean and standard deviation of the dML errors (denoted respectively as meanE and sdE), and the ratio of the area of the left hemisphere to that of the right hemisphere separated by the dML [11].

For quantifications, the position of P is the geometric center of the tumor, while the mass of P is the sum of voxels of tumor and edema on the axial slice with maximum MLS.

In this section, we show the quantification results of the proposed method, some relevant additional experimental results, and the contributing factors of tumor and edema to dML.

Performance evaluation

The dMLs of ground truth, the proposed method for two typical scans with different extents of edema are shown in Fig. 8.

Comparisons between the approximated and ground truth dMLs are measured as well for quantification. Specifically, the maximum value of the dML errors of the voxels on the approximated dML is adopted to quantify the error of the maximum distance of the proposed method, which is called the maximum distance error of the approximated dML. Similarly, the error of area ratio of the approximated dML is the absolute difference between the ratios calculated by approximated and ground truth dML. The scatter plot of MLS (approximated and ground truth) and the error distribution are shown respectively in Figs. 9 and 10. The distributions of the maximum distance errors,

area ratio errors, Mean_sim, and sd_sim of the 30 data are summarized in Table 2.

Performance comparison using different local symmetry metrics

To see the accuracy dependency on four ways of local symmetry: SD, SS, SG, and Sym, experiments are carried out for all the 30 subjects. The approximated dMLs using SD, SS, SG, and Sym are shown in Fig. 11 for a scan with large MLS, while the statistics of the accuracy are summarized in Table 3.

Paired t-tests have been carried out to see if the proposed method with four local symmetries will have significantly different accuracies. The maximum distance error, area ratio error, meanE and sdE with Sym are significantly smaller than those of SD, all with $p \leq 0.002$. Compared with SS and SG, the proposed method with Sym has significantly smaller meanE ($p = 0.003$ and $p < 0.001$) and sdE (both $p = 0.001$).

Discussion

A midline, which is the border between the left and right hemispheres, is a feature requiring a large number of voxels to compute regardless of being deformed or not. For the cases without deformation, midlines could be approximated as a plane and attained through exploring local symmetry and outlier removal [18]. However, it becomes challenging to calculate in case of deformation due to the following reasons:

(a) The shape of a midline is hard to predict;
(b) The grayscales on a midline can change substantially as it may contain cerebrospinal fluid, gray matter, white matter, and voxels with pathology such as tumor and edema, and
(c) The symmetry might be destroyed due to the deformation of the lesion.

Table 1 The procedure to approximate dML

Step 1	Compute the composite local symmetry metric
Step 2	Assign the initial modulation factor A in Eq. (4) in range $[5 \times 10^{-5}, 4.5 \times 10^{-3}]$ and the iteration step with 1×10^{-5}
Step 3	Predict the dML using Eq. (6)
Step 4	Calculate the sum of the local symmetry of the voxels on the predicted dML
Step 5	Record the predicted dML with maximum sum value from step 4 and return to step 3 until all A has been checked
Step 6	Refine the predicted dML according to local symmetry and smooth the curve

Fig. 8 The ground truth of dML(*blue curve*) (**a**), the lesions segmented manually with four labels for different pathologies (from *dark* to *bright*): necrosis, edema, non-enhanced tumor and enhanced tumor (**b**), and the estimated dML by the proposed method of two typical data

(a)   **(b)**   **(c)**
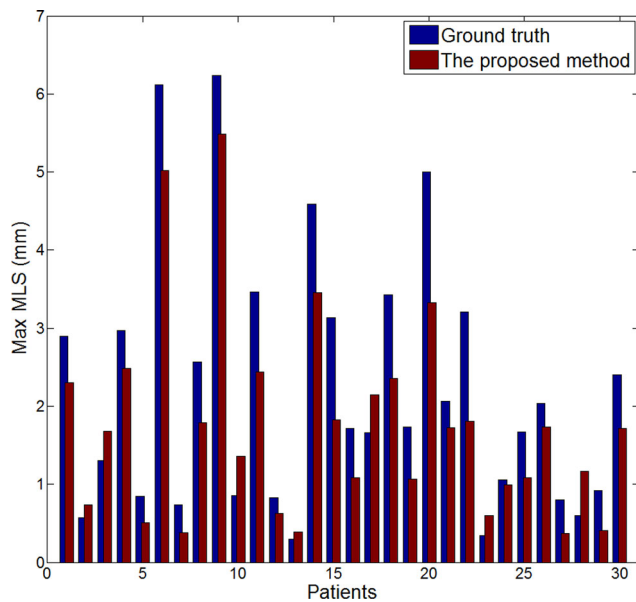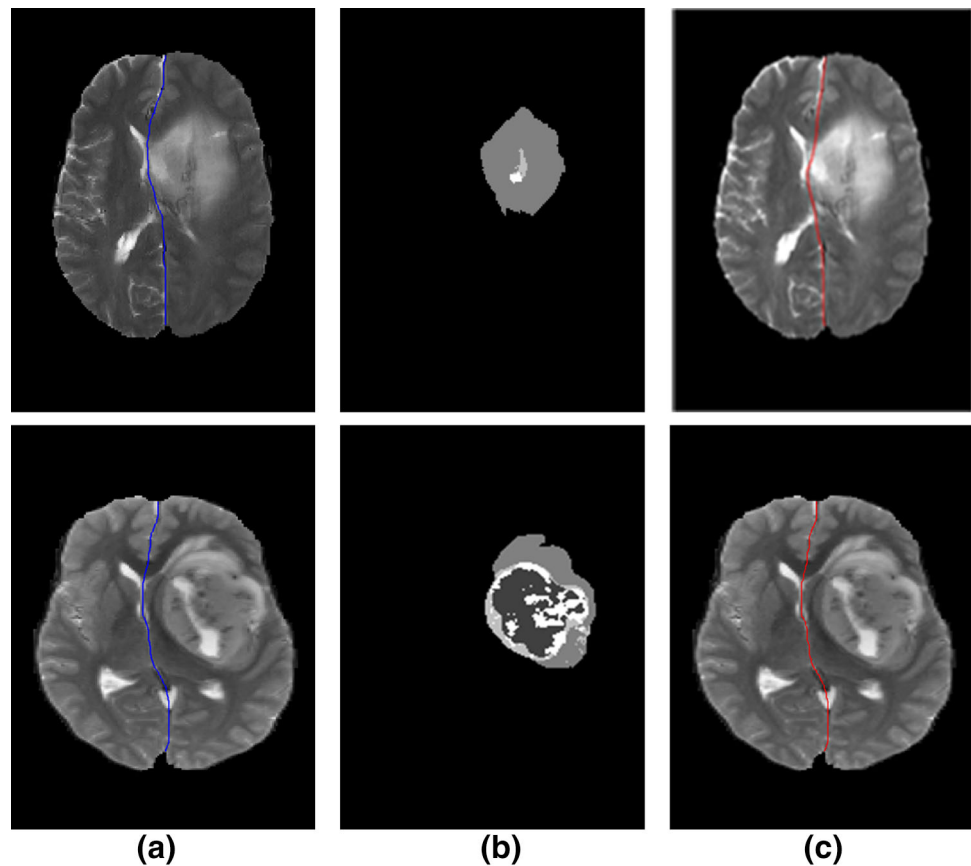
**Fig. 9** The *scatter plot* of MLS: approximated and ground truth

The axial slice with maximum MLS is most relevant for clinical implications and is picked manually for quantification, which is a tedious procedure to be automated. We checked closely these 30 data sets and summarized the following rule that was applicable to these 30 data sets. The rule may need more investigation to be generalized. Here the pathology-brain ratio of an axial slice is defined as the ratio of the number of pathology voxels to the number of brain voxels within the axial slice, and pathology could be either tumor or edema. For each of the 30 data sets, the axial slice with the maximum tumor-brain ratio could be found, and the axial slice with the maximum edema-brain ratio could also be found; these two maximum pathology-brain ratios are compared to pick the axial slice with the bigger pathology-brain ratio as the representative axial slice.

Extraction of feature points that are supposed to be on the midline such as falces and SP sounds good, but these points are too sparse for an accurate determination of the midline, let alone the difficulty and possible errors to determine these feature points. In this regard, the proposed method has an inherent advantage as it is based on calculating the deformation of all the points on the iML and does not assume the existence of any anatomical markers.

From Fig. 11 and Table 3, it can be seen that: (a) SS performs better than the traditional local intensity symmetry SD as adopted by Liao et al. [1], (b) SG performs better than SS, and (c) Sym performs substantially better

Fig. 10 The error distribution of 30 subjects
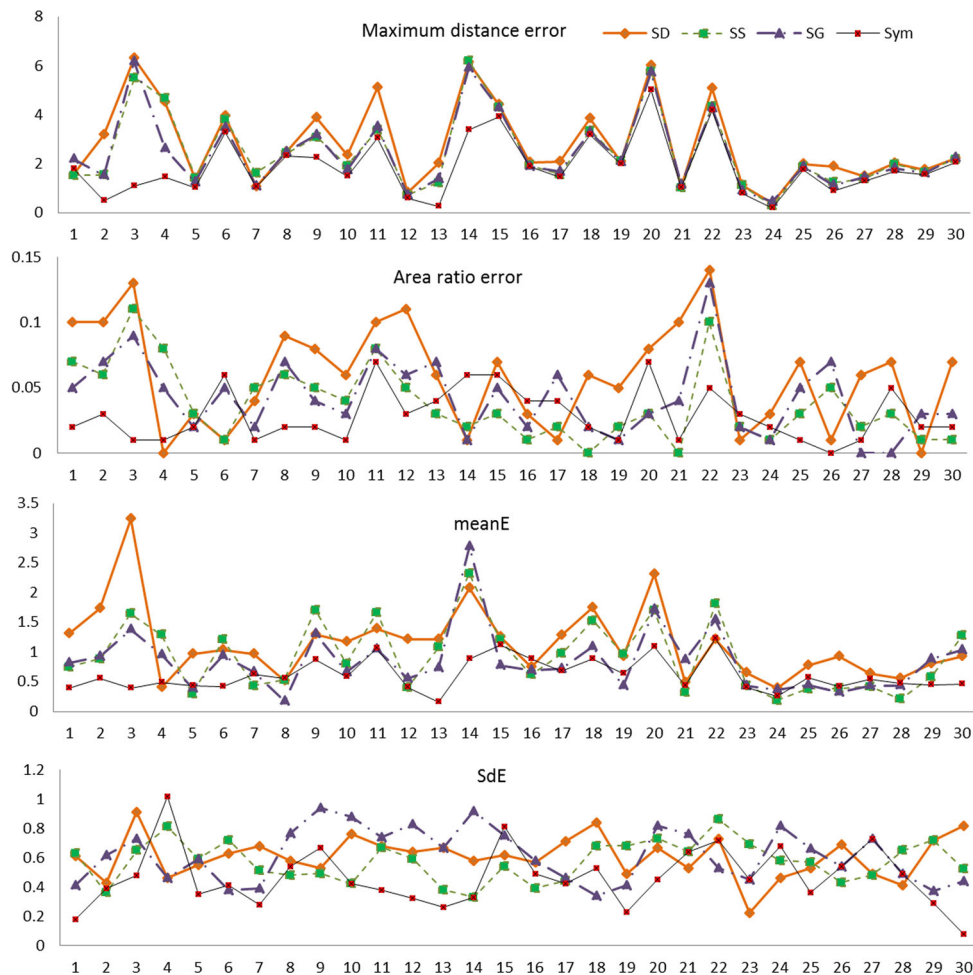
Table 2 Statistics of the errors between the approximated and ground truth dMLs

	Mean	SD
E_1 (mm)	1.89	1.18
E_2	0.03	0.02
E_3 (mm)	0.61	0.27
E_4 (mm)	0.46	0.20

E_1 for maximum distance error, E_2 for area ratio error, E_3 for meanE, E_4 for sdE, SD for standard deviation

than SS and SG, which may mean that SG and SS provide complementary information to locate dML.

An additional experiment has been carried out to see the relationship between the MSL accuracy and the interpolated spatial resolution. Seven interpolated spatial resolutions of a patient are used to compare the accuracy and time consumption. As the result shown (Fig. 12; Table 4), decreasing the voxel size from 1 to 0.2 mm via bicubic interpolation can decrease the maximum distance error (E_1) from 2.94 mm to at most 1.45 mm, but E_1 will not change much from spatial resolution of 0.4 mm (spatial amplification of 2.5 × 2.5) while the time consumed can increase substantially. The error will not take the minimum value at the highest spatial resolution. It seems that a spatial amplification of 3 × 3 could attain a good trade-off between accuracy and time consumption (with $E_1 = 1.45$ mm and time = 15.42 s).

A comparative experiment has been carried out to compare the performance of simple curve smoothing and B-spline curve fitting. Simple curve smoothing was preferred as it yielded a smaller average E_1 (1.89 mm) than the curve fitting ($E_1 = 1.91$).

Tumor and cerebral edema are the major contributing factors to MLS through mass effect. In our model, these two factors will impact the dML through the geometrical center P and the pathological region (Fig. 2). To see the influence of *P*, we carry out experiments with the

Fig. 11 dML of ground truth (*blue curve*) (**a**), dML of the proposed method with composite local symmetry Sym (*red curve*) (**b**), SD (*green curve*) (**c**), SS (*yellow curve*) (**d**), and SG (*purple curve*) (**e**) of a subject
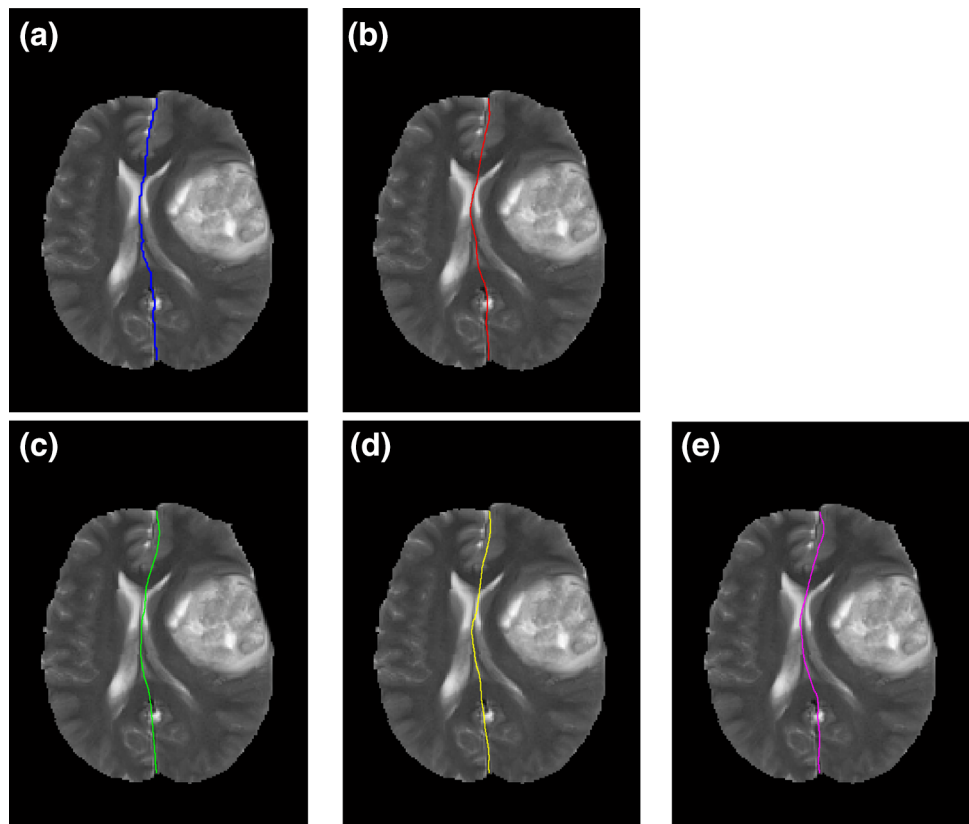

Table 3 Accuracy dependency of the approximated dMLs on four ways to defined the local symmetry for all the 30 subjects

	SD		SS		SG		Sym	
	Mean	SD	Mean	SD	Mean	SD	Mean	SD
E_1 (mm)	2.82	1.66	2.52	1.55	2.44	1.51	1.89	1.18
E_2	0.06	0.04	0.04	0.03	0.04	0.03	0.03	0.02
E_3 (mm)	1.14	0.60	0.94	0.57	0.85	0.51	0.61	0.27
E_4 (mm)	0.61	0.14	0.57	0.13	0.62	0.18	0.46	0.20

pathological region fixed (to be the whole lesion) while changing the P to be the geometrical center of tumor, edema, and the whole lesion respectively (Fig. 13). Experiments are also carried out to see the influence of pathological region by fixing P (to be the geometric center of tumor) while varying the pathological region to be respectively the tumor, edema, and the whole lesion (Fig. 14). Quantification of these experiments is summarized in Tables 5 and 6.

Fig. 12 The accuracy versus the spatial amplification of a patient data
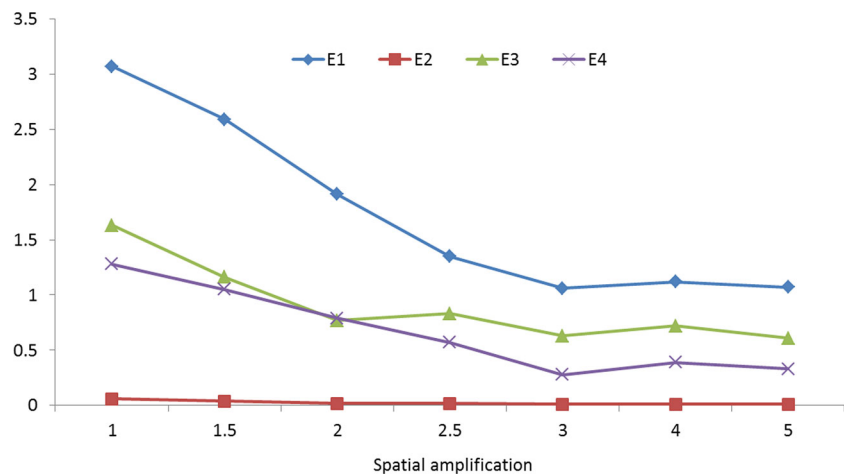
Table 4 Accuracy dependence on the interpolated spatial resolution of a patient data with different spatial resolutions via bicubic interpolation

	E$_1$ (mm)	E$_2$	E$_3$ (mm)	E$_4$ (mm)	Time (s)
Original	3.07	0.06	1.63	1.28	3.79
1.5 × 1.5	2.59	0.04	1.16	1.05	6.18
2 × 2	1.91	0.02	0.77	0.79	8.53
2.5 × 2.5	1.35	0.02	0.83	0.57	11.09
3 × 3	1.06	0.01	0.63	0.28	16.24
4 × 4	1.12	0.01	0.72	0.39	25.03
5 × 5	1.07	0.01	0.61	0.33	31.88

The proposed method will yield better accuracy with P being the geometric center of tumor (Fig. 13; Table 5) and the pathological region being the whole lesion (Fig. 14; Table 6). This may imply that the size of the whole lesion and the location of tumor (instead of edema or the sum of edema and tumor) are more appropriate to determine the extent of deformation. The mechanism of deformation will need more investigation.

Below is a summarization of the major contributions of this study.

(a) An enhanced Voigt model to relate the deformation of midline to the size and position of lesions for dML prediction to reflect the viscoelasticity of tissues on dML.

(b) A new way to calculate the local symmetry in the vicinity of dML has been proposed by combining the local intensity symmetry and local intensity gradient symmetry. In this way, the dML voxels within the uniform regions could be better differentiated than the traditional local intensity symmetry. The new way of quantifying local symmetry around dML makes the dML refinement more accurate (Table 3).

(c) For the cases with large deformation, where the traditional local symmetry around dML is destroyed or the anatomical markers are missing (Fig. 8a), the proposed method could still perform well as it is based on mechanical model and composite local symmetry, while existing methods [1, 6–11] based on the existence of anatomical markers will fail.

Fig. 13 Estimation of dML based on the proposed method with different geometric center P and fixed pathological region: the ground truth dML (*blue curve*) (**a**), the ground truth lesions (from *dark* to *bright*: necrosis, edema, non-enhancing tumor and enhanced tumor) (**b**), dML from P being the geometric center of tumor (**c**), dML from P being the geometric center of edema (**d**), and dML from P being the geometric center of the whole lesion (**e**)
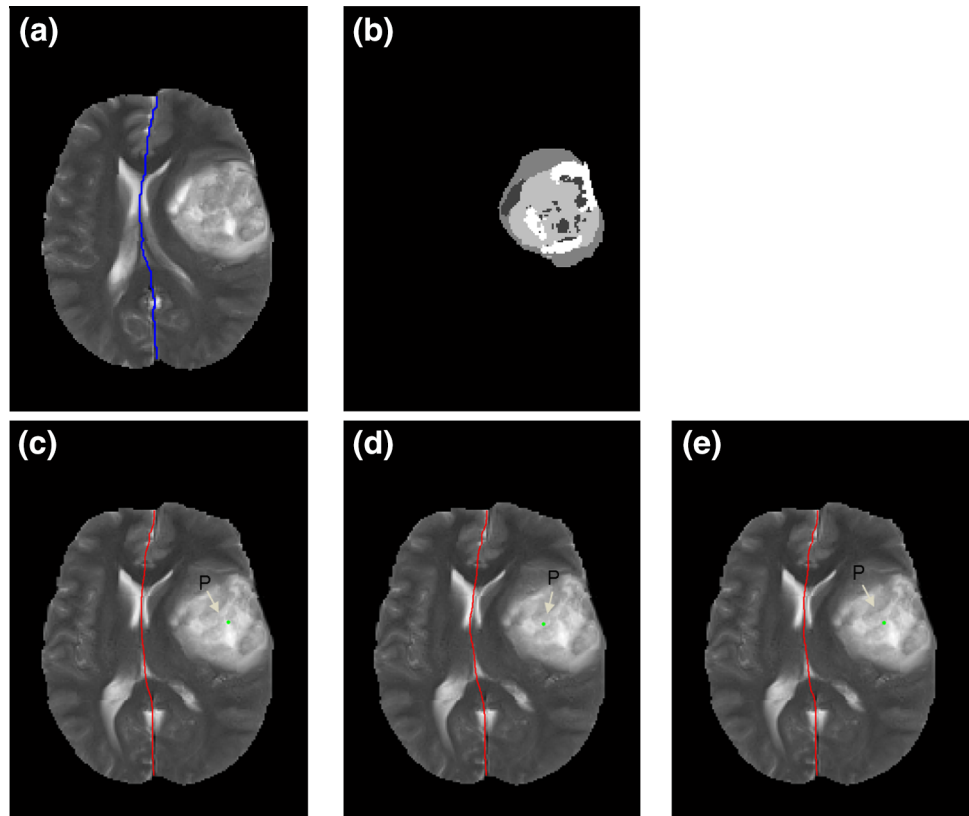
Fig. 14 Estimation of dML based on proposed method with fixed *P* but varying pathological regions: ground truth dML (*blue curve*) (**a**), dML from the whole lesions (*red curve*) (**b**), dML from the tumor (*purple curve*) (**c**), dML from the edema (*green curve*) (**d**), and (**e**) dML form the edema plus tumor (*yellow curve*)
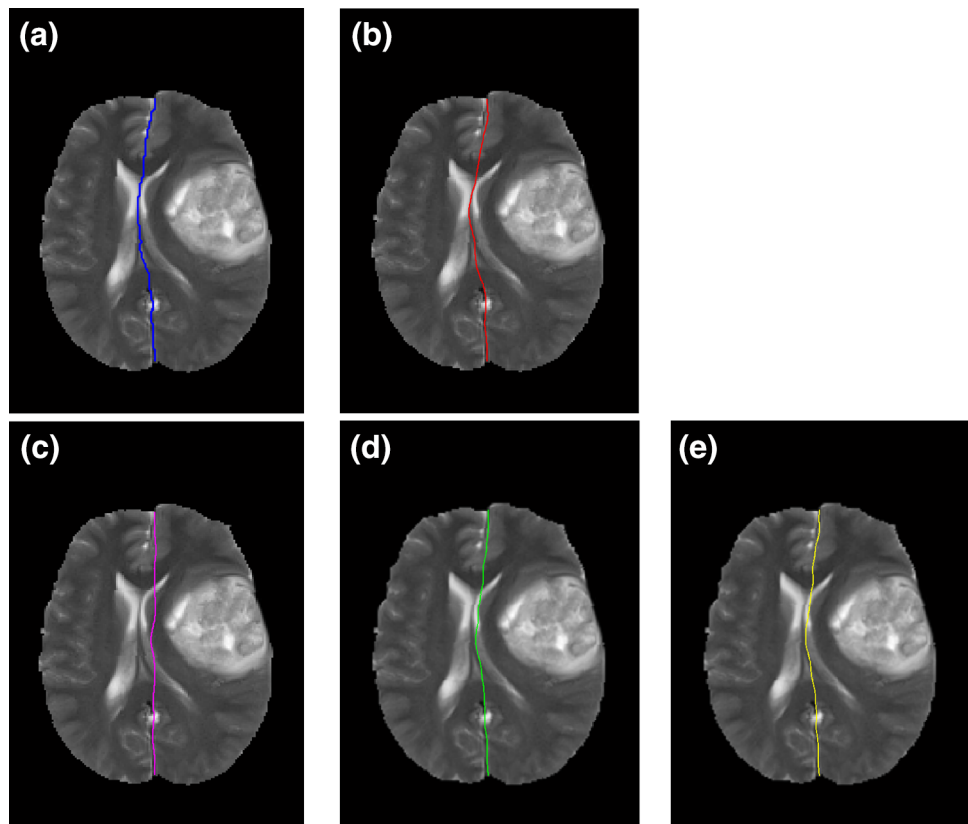
Table 5 Quantification of the experiments using different geometric centers

	E_1 (mm)	E_2	E_3 (mm)	E_4 (mm)
Tumor	1.06	0.01	0.63	0.28
Edema	1.33	0.02	0.72	0.51
Whole lesion	1.31	0.01	0.66	0.42

Table 6 Quantification of the experiments using different pathological regions

|	E_1 (mm)	E_2	E_3 (mm)	E_4 (mm)
Tumor only	1.79	0.02	0.65	0.94
Edema only	3.75	0.05	1.37	1.21
Tumor plus edema	1.58	0.02	0.84	1.06
Whole lesion	1.06	0.01	0.63	0.28

(d) The proposed methodology has been exploited to investigate the contribution of different pathologies after glioma, which may be employed as a methodological tool for deformation study of MRI scans.

The proposed method could not handle well cases when a large portion of dML is occupied by lesions. Figure 15 shows two scans of low- and high-grade gliomas with the maximum error. In these cases, the portion of dML occupied by lesions is even difficult to be manually delineated by experienced radiologists.

As the proposed method approximates the dML on each voxel, it could be explored for estimating midsagittal surface which could be useful for registration and quantifying the brain.

Conclusion

To the best of our knowledge, for delineation of deformed midline, this is the first report on both quantification of gliomas and delineation from MRI, which hopefully will provide valuable information for diagnosis and therapy. The study suggests that the size of the whole lesion and the location of tumor (instead of edema or the sum of edema and tumor) could be more appropriate to determine the extent of deformation. Composite local symmetry is recommended to represent the local symmetry around the dML. The proposed method could be potentially used to quantify the severity of patients with cerebral gliomas and
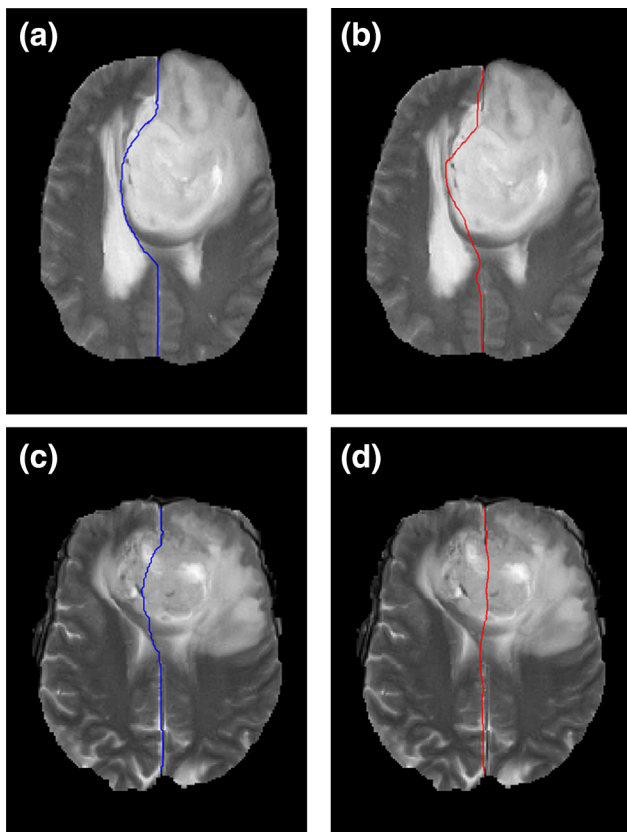
Fig. 15 Two cases with maximum error of the proposed method: the ground truth and the estimated dMLs for low- (**a** and **b**) and high-grade (**c** and **d**) gliomas

other brain pathology, as well as to approximate mid-sagittal surface for brain quantification.

Compliance with ethical standards

Conflict of Interest   The authors declare that they have no conflict of interest.

Ethical approval   All procedures performed in studies involving human participants were in accordance with the ethical standards of the institutional and/or national research committee and with the 1964 Helsinki declaration and its later amendments or comparable ethical standards.

Informed consent   For this type of retrospective studies, formal consent is not required. Informed consent was obtained from all individual participants included in the study.

References

1. Liao C, Xiao I, Wong J (2006) Tracing the deformed midline on brain CT. Biomed Eng-App Bas C 18(6):305–311
2. Legler JM, Ries LAG, Smith MA, Warren JL, Heineman EF, Kaplan RS, Linet MS (1999) Brain and other central nervous system cancers: recent trends in incidence and mortality. J Natl Cancer I 91(16):1382–1390
3. Olson JD, Riedel E, DeAngelis LM (2000) Long-term outcome of low-grade oligodendroglioma and mixed glioma. Neurology 54(7):1442–1448
4. Gamburg ES, Regine WF, Patchell RA, Strottmann JM, Mohiuddin M, Young AB (2000) The prognostic significance of midline shift at presentation on survival in patients with glioblastoma multiforme. Int J Radiat Oncol 48(5):1359–1362
5. Papadopoulos MC, Saadoun S, Binder DK, Manley GT, Krishna S, Verkman AS (2004) Molecular mechanisms of brain tumor edema. Neuroscience 129(4):1009–1018
6. Liu R, Li S, Chew L, Boon C, Tchoyosom C, Cheng K, Tian Q, Zhang Z (2009) From hemorrhage to midline shift: a new method of tracing the deformed midline in traumatic brain injury CT images. In: 16th IEEE international conference on image processing, pp 2637–2640
7. Xiao F, Chiang I, Wong J, Tsai Y, Huang K, Liao C (2011) Automatic measurement of midline shift on deformed brains using multiresolution binary level set method and Hough transform. Comput Biol Med 41(9):756–762
8. Xiao F, Liao C, Huang K, Chiang I, Wong J (2010) Automated assessment of midline shift in head injury patients. Clin Neurol Neurosur 112(9):785–790
9. Liao C, Xiao F, Wong J, Chiang I (2009) A multiresolution binary level set method and its application to intracranial hematoma segmentation. Comput Med Imag Grap 33(6):423–430
10. Chen W, Najarian K, Ward K (2010) Actual midline estimation from brain CT scan using multiple regions shape matching. In: 20th IEEE international conference on pattern recognition, pp 2552–2555
11. Liu R, Li S, Su B, Tan CL, Leong TY, Pang BC, Lim CCT, Lee CK (2014) Automatic detection and quantification of brain midline shift using anatomical marker model. Comput Med Imag Grap 38(1):1–14
12. Joseph DD (1990) Fluid dynamics of viscoelastic liquids, vol 84. Springer-Verlag, New York
13. Miller K, Chinzei K, Orssengo G, Bednarz P (2000) Mechanical properties of brain tissue in vivo: experiment and computer simulation. J Biomech 33(11):1369–1376
14. Klatt D, Hamhaber U, Asbach P, Braun J, Sack I (2007) Non-invasive assessment of the rheological behavior of human organs using multifrequency MR elastography: a study of brain and liver viscoelasticity. Phys Med Biol 52(24):7281
15. Sack I, Beierbach B, Wuerfel J, Klatt D, Hamhaber U, PapazoglouS Martus P, Braun J (2009) The impact of aging and gender on brain viscoelasticity. Neuroimage 46(3):652–657
16. Schiessel H, Metzler R, Blumen A, Nonnenmacher TF (1995) Generalized viscoelastic models: their fractional equations with solutions. J Phys-A-Math Gen 28(23):6567
17. Zhuang D, Liu Y, Wu J, Yao C, Mao Y, Zhang C, Wang M, Wang W, Zhou L (2011) A sparse intraoperative data-driven biomechanical model to compensate for brain shift during neuronavigation. Am J Neuroradiol 32(2):395–402
18. Hu Q, Nowinski WL (2003) A rapid algorithm for robust and automatic extraction of the midsagittal plane of the human cerebrum from neuroimages based on local symmetry and outlier removal. Neuroimage 20(4):2154–2166
19. Meyers MA, Krishan KC (2009) Mechanical behavior of materials. Cambridge University Press, Cambridge

20. Haslach HW Jr (2005) Nonlinear viscoelastic, thermodynamically consistent, models for biological soft tissue. Biomech Model Mechan 3(3):172–189
21. Miller K, Chinzei K (2002) Mechanical properties of brain tissue in tension. J Biomech 35(4):483–490
22. Davidson RJ, Hugdahl K (1996) Brain asymmetry. MIT Press/Bradford Books, Cambridge
23. Lindeberg T (1993) Scale-space theory in computer vision. Springer, New York
24. Zitnick CL, Ramnath K (2011) Edge foci interest points. In: IEEE international conference on computer vision, pp 359–366
25. Lowe DG (1999) Object recognition from local scale-invariant features. In: 7th IEEE international conference on computer vision, pp 1150–1157
26. Dalal N, Triggs B (2005) Histograms of oriented gradients for human detection. In: IEEE international conference on computer vision and pattern recognition, pp 886–893
27. Hauagge DC, Noah S (2012) Image matching using local symmetry features. In: IEEE international conference on computer vision and pattern recognition, pp 206–213